

## Supporting Information

# Ni Nanoparticles Decorated-MnO<sub>2</sub> Nanodendrites as High Selective and Efficient Catalysts for CO<sub>2</sub> Electroreduction

Xu-Jun He, Jin-Xian Feng, Qian Ren, and Gao-Ren Li\*

\*Email - ligaoren@mail.sysu.edu.cn

## Experimental Section

**Synthesis of Ni NPs/MnO<sub>2</sub> NDs-CFs:** In a typical procedure for synthesizing Ni NPs/MnO<sub>2</sub> NDs-CFs, the electrodeposition method was used, and all the experiments were carried out in a simple two-electrode cell by galvanostatic electrolysis. The graphite electrode was used as a counter electrode (spectral grade, 1.8 cm<sup>2</sup>), and the carbon fibers (CFs) (Phychemi Company, Hong Kong) were utilized as a working electrode (0.5 cm×2 cm). Anodic electrodeposition was performed at a constant current of 0.20 mA/cm<sup>2</sup> in the solution of 0.01 M Mn(CH<sub>3</sub>COO)<sub>2</sub> + 0.05 M CH<sub>3</sub>COONH<sub>4</sub> at 70 °C for 90 min. Ni nanoparticles were electrodeposited on MnO<sub>2</sub> NDs-CFs in solution of 0.01 M NiSO<sub>4</sub> + 0.02 M sodium citrate at 1.0 mA/cm<sup>2</sup> for 6 min at 30 °C.

**Synthesis of MnO<sub>2</sub> NDs-CFs:** In a typical procedure, the anodic electrodeposition was performed at a constant current of 0.2 mA/cm<sup>2</sup> in solution of 10 mL 0.01 M Mn(CH<sub>3</sub>COO)<sub>2</sub> + 0.05 M CH<sub>3</sub>COONH<sub>4</sub> at 70 °C for 90 min.

**Synthesis of Ni NPs-CFs:** In a typical procedure, Ni NPs were deposited on the surface of CFs to form Ni NPs-CFs by electrodeposition in solution of 15 mL 0.01 M NiSO<sub>4</sub> and 0.02 M sodium citrate at 1.0 mA/cm<sup>2</sup> for 6 min at 30 °C.

---

**Characterizations:** The purity and crystallinity of as-obtained samples were characterized by powder X-ray diffraction (XRD) on a Philips X'Pert Pro Super diffractometer using Cu  $K_\alpha$  radiation ( $\lambda = 1.54178 \text{ \AA}$ ). X-ray photoelectron spectra (XPS) were achieved on an ESCALAB MKII with Mg  $K\alpha$  ( $h\nu = 1253.6 \text{ eV}$ ) as the excitation source. The binding energies obtained in the XPS spectral analysis were corrected for specimen charging by referencing C 1s to 284.8 eV. Field emission scanning electron microscopy (FE-SEM) images were performed by using a FEI Sirion-200 SEM. Transmission electron microscopy (TEM) images and high-resolution TEM image were acquired by using a JEOL-2010 TEM with an acceleration voltage of 200 kV. The liquid products were quantified by  $^1\text{H}$  NMR (Bruker AVANCE AV III 400) spectroscopy, in which 0.5 mL electrolyte was mixed with 0.1 mL  $\text{D}_2\text{O}$  (deuterated water) and 0.05  $\mu\text{L}$  dimethyl sulfoxide (DMSO, Sigma, 99.99%) was added as an internal standard.  $\text{HCOO}^-$  content in the electrolyte is determined by liquid chromatography mass spectrometer (Shimadzu, analysis software: LCMS Solution 3.10). The samples were also characterized by Brunauer-Emmett-Teller (BET) oxygen and nitrogen sorption surface area measurements (Micromeritics ASAP 2010). The specific surface areas of the synthesized materials were calculated by the Brunauer-Emmett-Teller (BET) method.

All the electrochemical measurements were implemented in a three-electrode system at an electrochemical station (CHI 760D). The working electrode was Ni NPs/ $\text{MnO}_2$  NDs-CFs. The graphite rod and the saturated calomel electrode (SCE) reference electrode served as the counter and reference electrodes, respectively. For  $\text{CO}_2$  reduction experiments, linear sweep voltammetry with a scan rate of 5 mV/s was carried out in  $\text{CO}_2$ -saturated 0.1 M  $\text{KHCO}_3$  solution (60 mL) (The  $\text{KHCO}_3$  electrolyte was purged with  $\text{CO}_2$  for 30 min prior to the measurement). The potential, measured against a SCE electrode, was converted to the potential versus reversible hydrogen electrode (RHE) according to  $E(\text{RHE}) = E(\text{SCE}) + E_0(\text{SCE}) + 0.059 \text{ pH}$ .

---

TOF values were calculated using Equation (1).<sup>[4-6]</sup>

$$\text{TOF}(\text{s}^{-1}) = (j \times A) / (2 \times F \times n) \quad (1)$$

Here,  $j$  ( $\text{mA cm}_{\text{geo}}^{-2}$ ) is the measured current density at a definite overpotential,  $A$  ( $\text{cm}_{\text{geo}}^{-2}$ ) is the surface area of the electrocatalysts, the number 2 means 2 electrons to reduce one mole of  $\text{CO}_2$ ,  $F$  is Faraday's constant ( $96485.3 \text{ C/mol}$ ), and  $n$  is the moles of electrochemical materials on the electrode calculated from  $m$  and the molecular weight of the coated catalysts.

To acquire the ECSA of the working electrodes, their roughness factor ( $R_f$ ) should be obtained firstly according to the equation:  $\text{ECSA} = R_f S$ , where  $S$  was generally equal to the geometric area of glassy carbon electrode (In this work,  $S = 1.13 \text{ cm}^2$ ). The  $R_f$  was determined by the relation  $R_f = C_{\text{dl}} / 60 \mu\text{F cm}^{-2}$  based on the double-layer capacitance ( $C_{\text{dl}}$ ) of a smooth oxide surface ( $60 \mu\text{F cm}^{-2}$ ).<sup>7</sup> where the  $C_{\text{dl}}$  could be acquired by cyclic voltammetry measurement under the potential windows of  $-0.3 \sim -0.2 \text{ V}$  vs. SCE ( $0.1 \text{ M KHCO}_3$  solution). The scan rates were  $2 \text{ mV/s}$ ,  $5 \text{ mV/s}$ ,  $10 \text{ mV/s}$ ,  $20 \text{ mV/s}$ ,  $50 \text{ mV/s}$  and  $100 \text{ mV/s}$ . The  $C_{\text{dl}}$  was estimated by plotting the  $j_a - j_c$  at  $-0.25 \text{ V}$  (where  $j_c$  and  $j_a$  are the cathodic and anodic current densities, respectively) versus SCE against the scan rate, in which the slope was twice that of  $C_{\text{dl}}$ .

The Faradaic efficiency of formate was estimated from the ratio of the total amount of charge  $Q(\text{C})$  passed through the sample and the total amount of formate produced  $n$  formate (mol).  $Q = I \times t$ , where  $I(\text{A})$  refers to the reduction current at a specific applied potential,  $t$  is the time (s) for the constant reduction current. Assuming that two electrons are needed to produce one formate, the Faradaic efficiency can be calculated as follows:  $\text{Faradaic efficiency}/\% = 2F \times n_{\text{formate}} / Q = 2F \times n_{\text{formate}} / (I \times t)$ , where  $F$  is the Faraday constant,  $96480 \text{ C/mol}$ .

**Calculation details:** All the calculations were performed based on spin-polarized periodic density

---

functional theory (DFT) implemented in Gaussian 09 W.<sup>[1]</sup> The electron interactions were described by the projector augmented wave (PAW) method and the electron exchange and correlation energy were treated with the gradient corrected Perdew-Burke-Ernzerh (GGA-PBE) functional.<sup>[2]</sup> The kinetic cutoff energy for plane-wave basis set was set to be 400 eV. The total energy convergence was set to be lower than  $10^{-5}$  eV, and the force convergence was set to be smaller than 0.02 eV/Å. The dipole corrections were also used to the slab exposed (110) surface.

## References

1. M. J. Frisch, G. W. Trucks, H. B. Schlegel, G. E. Scuseria, M. A. Robb, J. R. Cheeseman, J. A. Montgomery, Jr., T. Vreven, K. N. Kudin, J. C. Burant, J. M. Millam, S. S. Iyengar, J. Tomasi, V. Barone, B. Mennucci, M. Cossi, G. Scalmani, N. Rega, G. A. Petersson, H. Nakatsuji, M. Hada, M. Ehara, K. Toyota, R. Fukuda, J. Hasegawa, M. Ishida, T. Nakajima, Y. Honda, O. Kitao, H. Nakai, M. Klene, X. Li, J. E. Knox, H. P. Hratchian, J. B. Cross, C. Adamo, J. Jaramillo, R. Gomperts, R. E. Stratmann, O. Yazyev, A. J. Austin, R. Cammi, C. Pomelli, J. W. Ochterski, P. Y. Ayala, K. Morokuma, G. A. Voth, P. Salvador, J. J. Dannenberg, V. G. Zakrzewski, S. Dapprich, A. D. Daniels, M. C. Strain, O. Farkas, D. K. Malick, A. D. Rabuck, K. Raghavachari, J. B. Foresman, J. V. Ortiz, Q. Cui, A. G. Baboul, S. Clifford, J. Cioslowski, B. B. Stefanov, G. Liu, A. Liashenko, P. Piskorz, I. Komaromi, R. L. Martin, D. J. Fox, T. Keith, M. A. Al-Laham, C. Y. Peng, A. Nanayakkara, M. Challacombe, P. M. W. Gill, B. Johnson, W. Chen, M. W. Wong, C. Gonzalez, J. A. Pople, *Gaussian*, Inc., Pittsburgh PA, 2009.
2. J. Tomasi, B. Mennucci, R. Cammi, *Chem. Rev.* 2013, **105**, 2999.
3. A. Reed, F. Weinhold, *J. Chem. Phys.* 1983, **78**, 4066.
4. C. Morales-Guio, M. Mayer, A. Yella, S. Tilley, M. Gratzel, X. Hu, *J. Am. Chem. Soc.* 2015, **137**, 9927.
5. X. Long, K. Li, S. Xiao, K. Yan, Z. Wang, H. Chen, S. Yang, *Angew. Chem. Int. Ed.* 2014, **53**, 7584.
6. M. Gao, W. Sheng, Z. Zhuang, Q. Fang, S. Gu, J. Jiang, Y. Yan, *J. Am. Chem. Soc.* 2014, **136**, 7077.
7. B. Cui, H. Lin, J. B. Li, X. Li, J. Yang, J. Tao, *Adv. Funct. Mater.* 2008, **18**, 1440-1447.

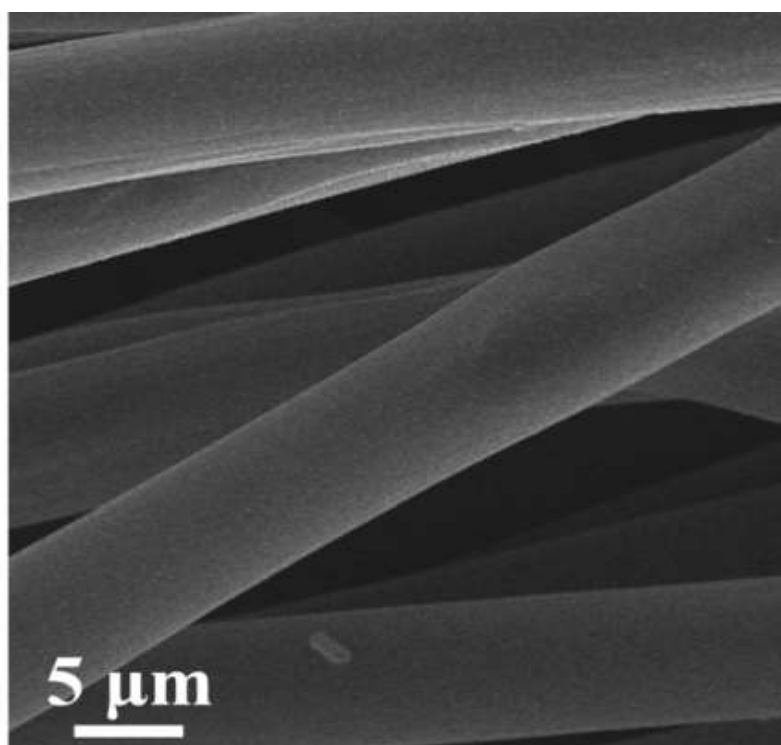


**Figure S1** SEM image of pristine CFs.

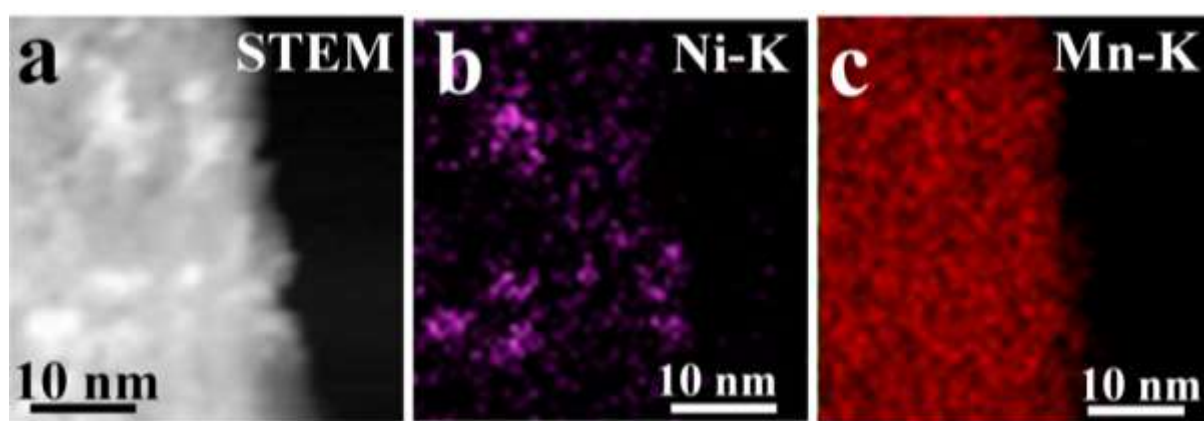


**Figure S2.** STEM-EDS mapping images of (a) STEM image of a part of Ni NPs/MnO<sub>2</sub> NDs, (b) EDS elemental mapping of Ni-K, and (c) Mn-K.

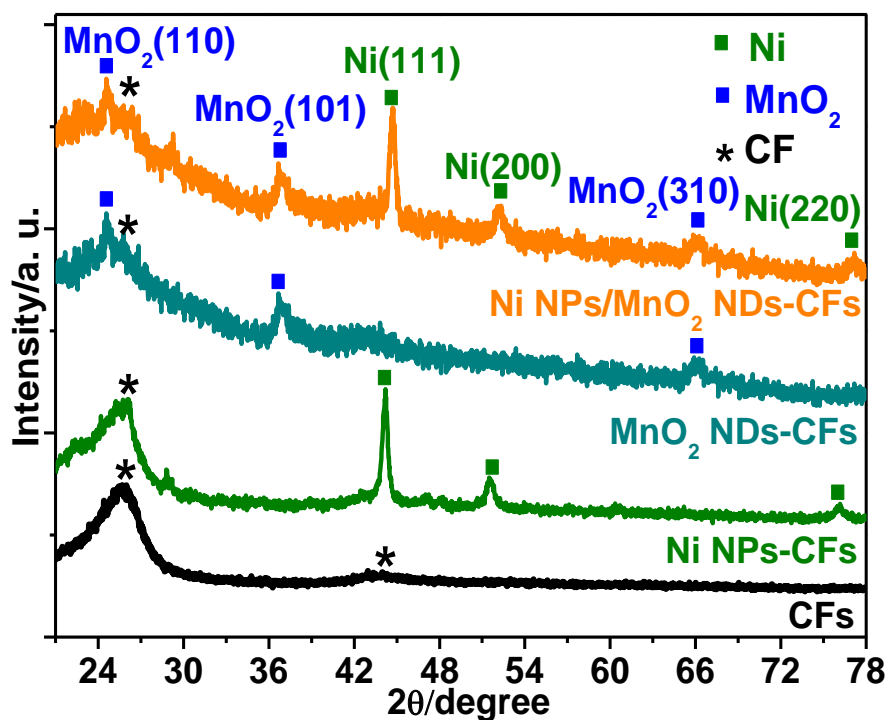


**Figure S3.** XRD patterns of the CF, Ni NPs-CF, MnO<sub>2</sub> NDs-CFs and Ni NPs/MnO<sub>2</sub> NDs-CFs.

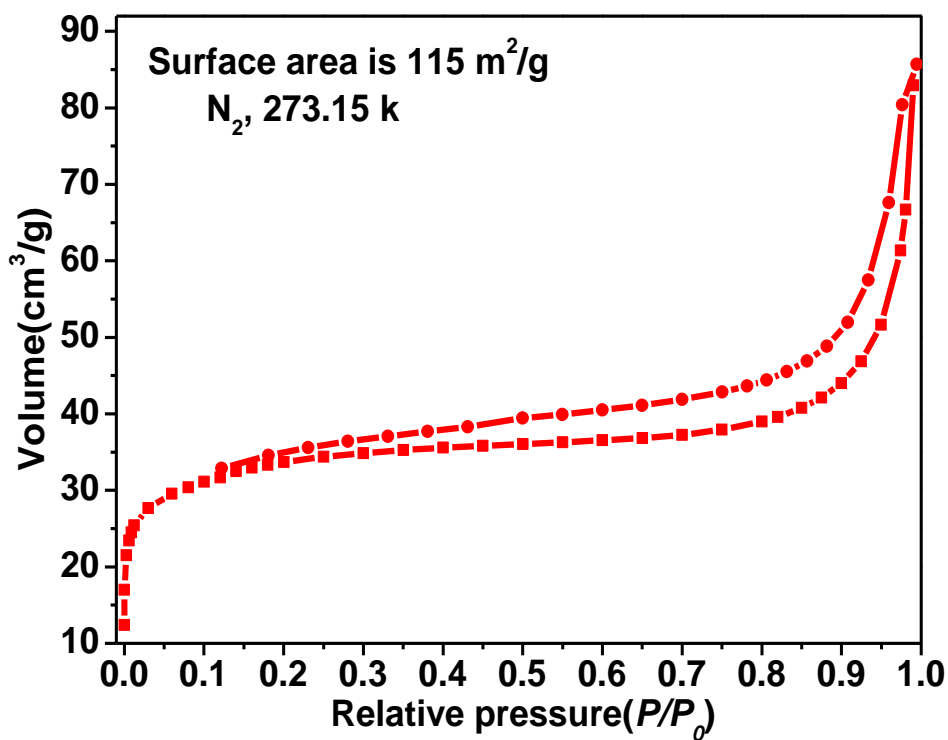


**Figure S4.** BET curve and surface area of Ni NPs/MnO<sub>2</sub> NDs.

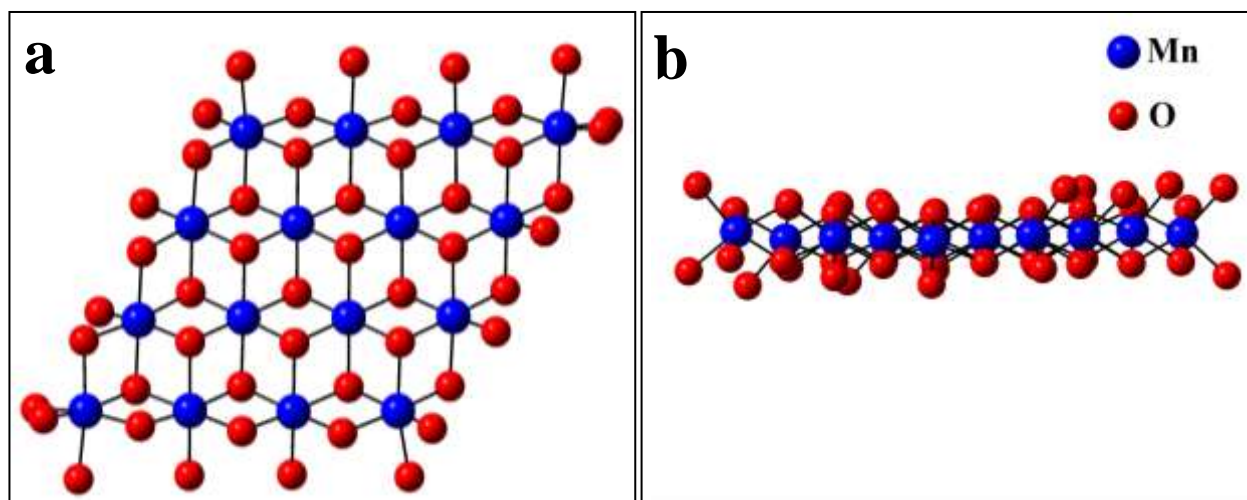


**Figure S5.** The optimized simplified structure of  $\text{MnO}_2$  cluster. (a) Top view; (b) side view.

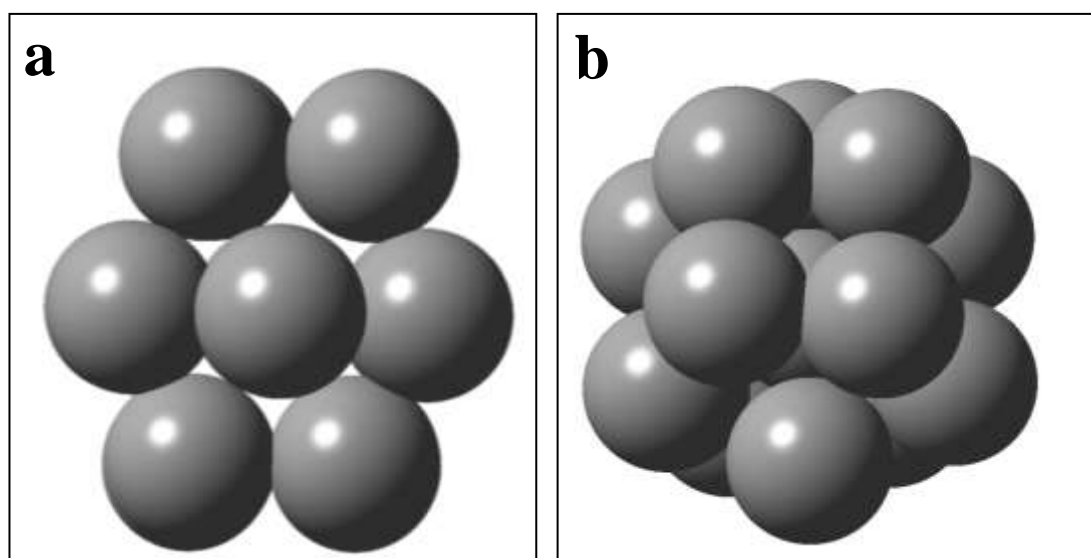


**Figure S6.** The optimized simplified structure of Ni cluster (a) Top view; (b) side view.

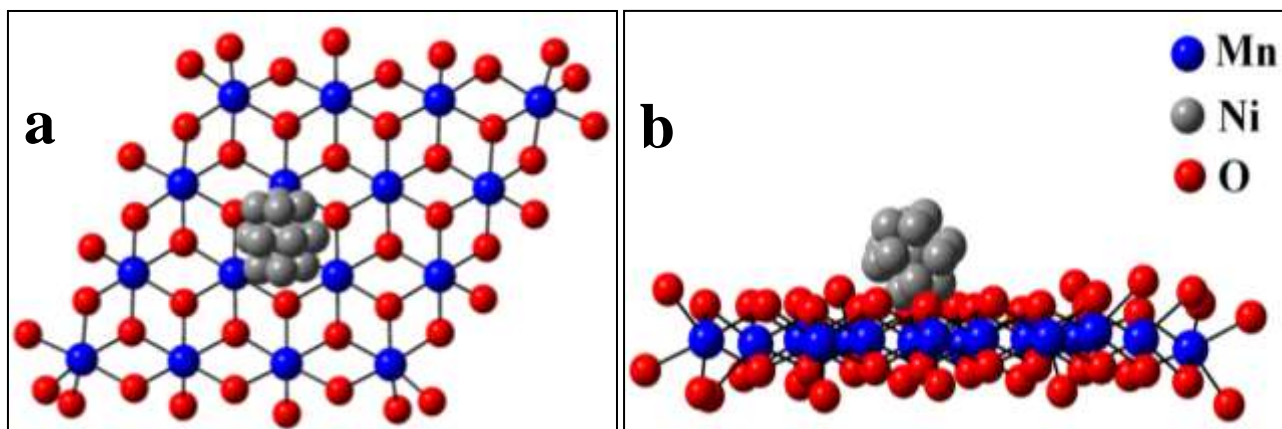


**Figure S7.** Optimized simplified structure of  $\text{MnO}_2/\text{Ni}$  cluster (a) Top view; (b) side view.

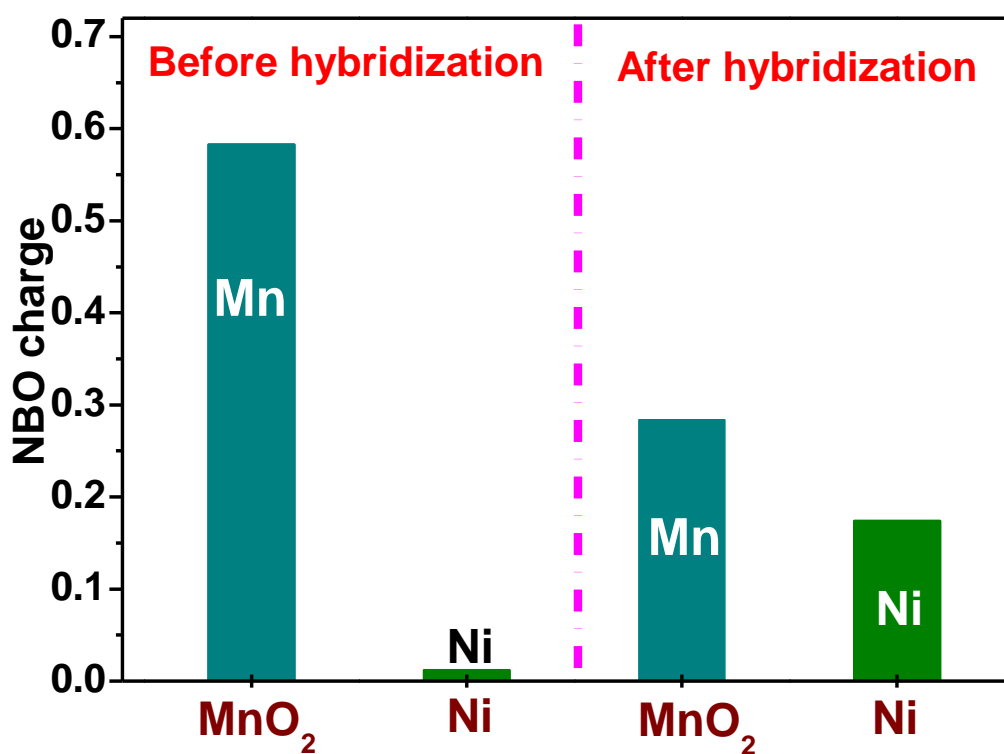


**Figure S8.** NBO charge distribution of Mn and Ni before and after hybridization.



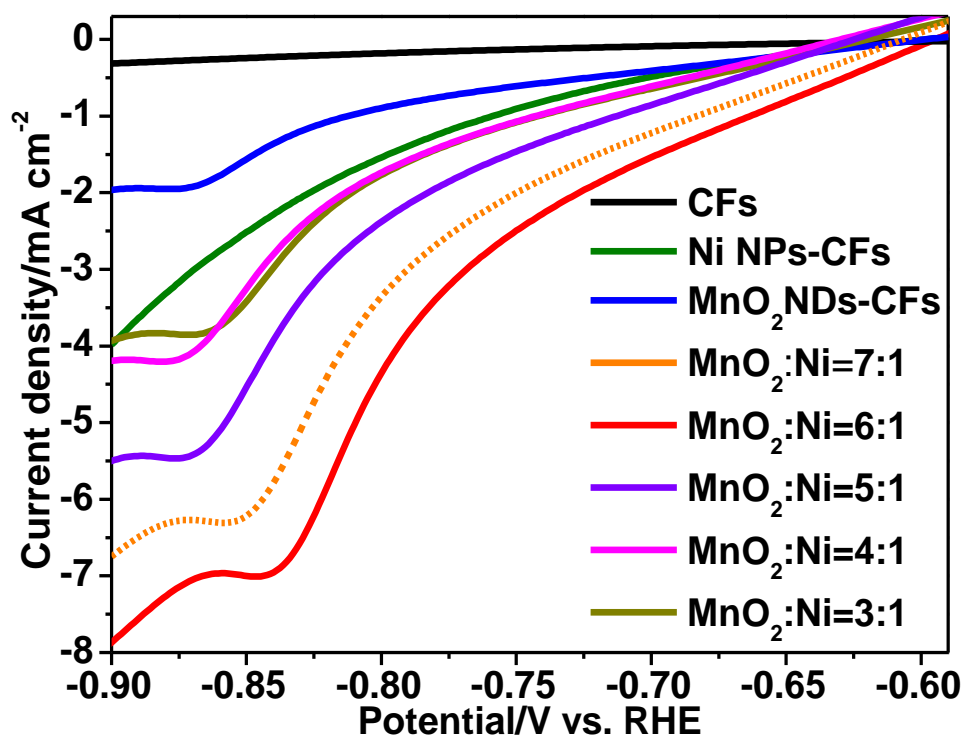


**Figure S9.** Polarization curves of Ni NPs/MnO<sub>2</sub> NDs-CFs with different mass ratio of MnO<sub>2</sub> and Ni.

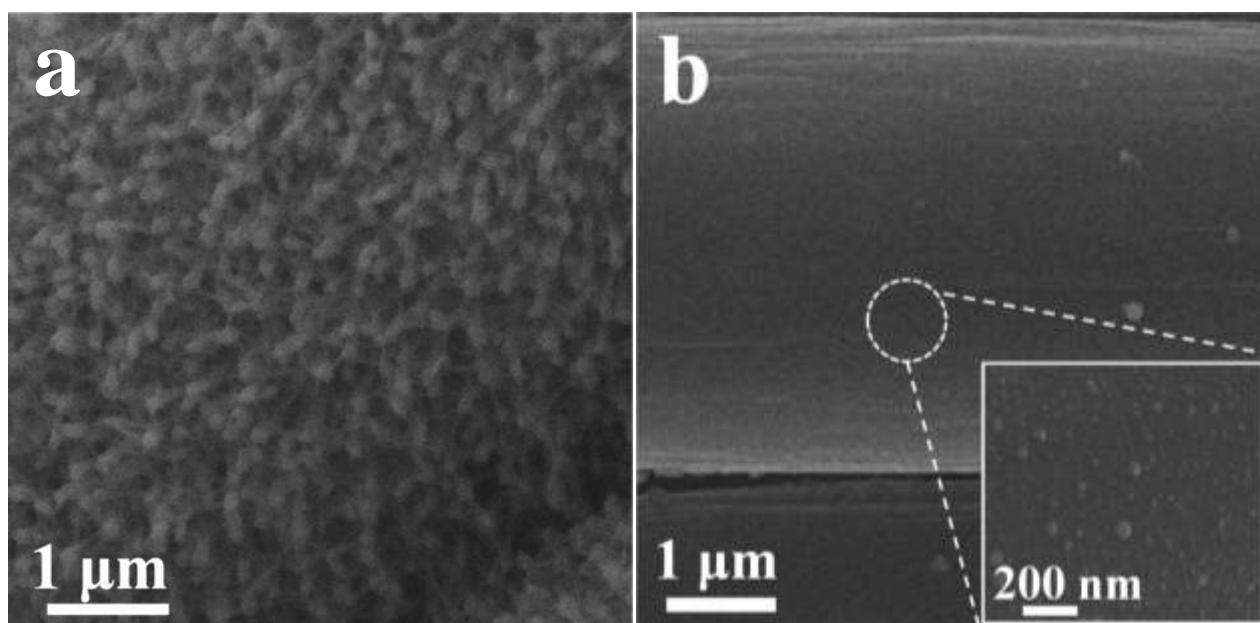


**Figure S10.** SEM images of (a) MnO<sub>2</sub> NDs-CFs; (b) Ni NPs-CFs.

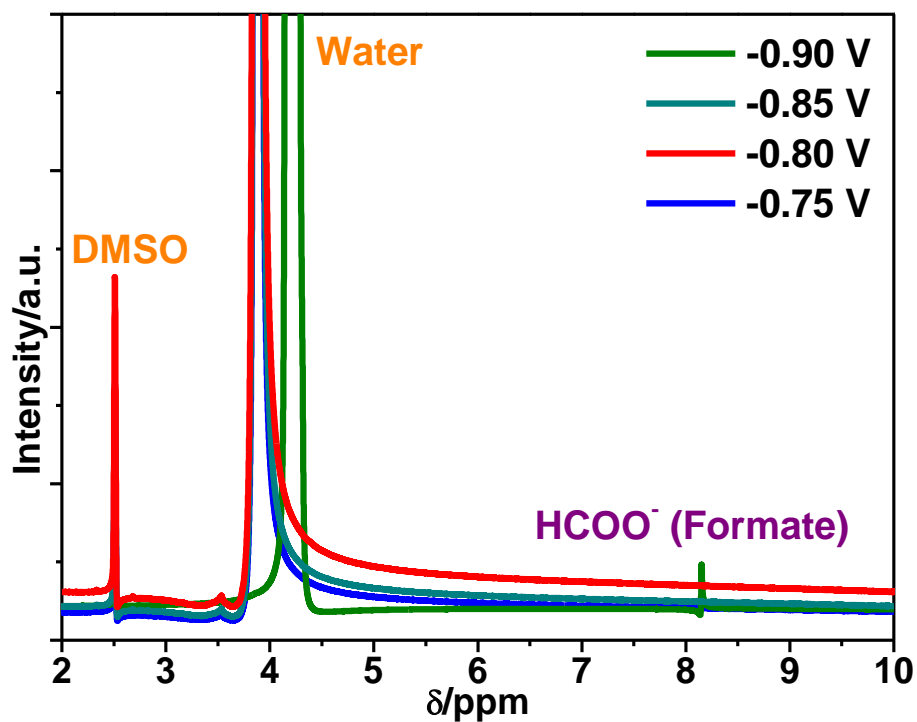


**Figure S11.**  $^1\text{H}$  NMR spectra of the electrolyte after  $\text{CO}_2$  reduction by Ni NDs-CFs at the potential from -0.75 to -0.90 V.

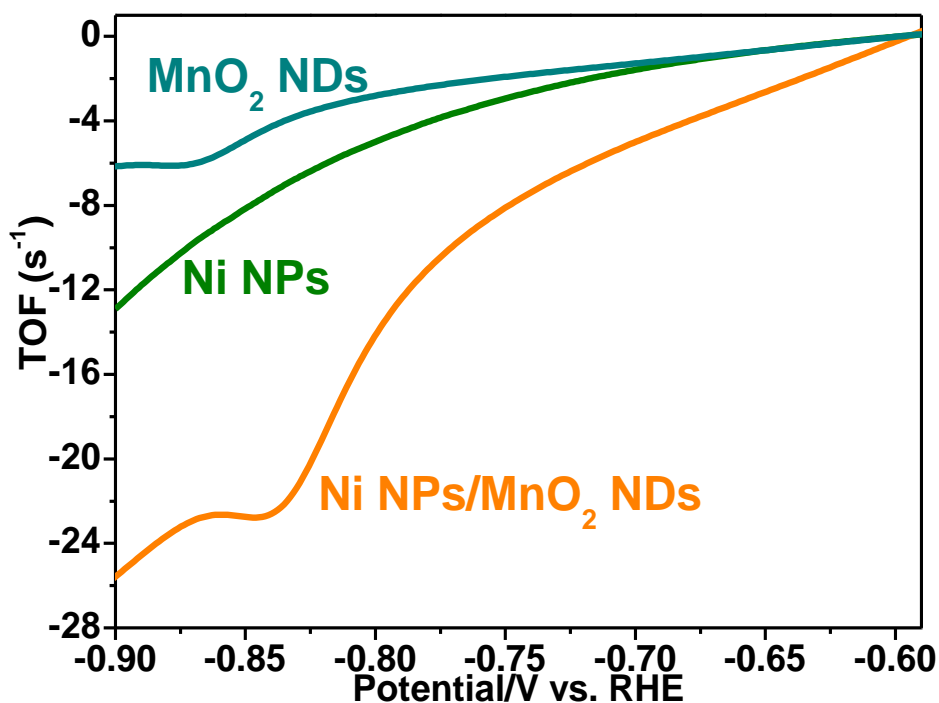


**Figure S12.** TOFs of Ni NPs/ $\text{MnO}_2$  NDs-CFs,  $\text{MnO}_2$  NDs-CFs, Ni NPs-CFs and CFs as a function of overpotential.

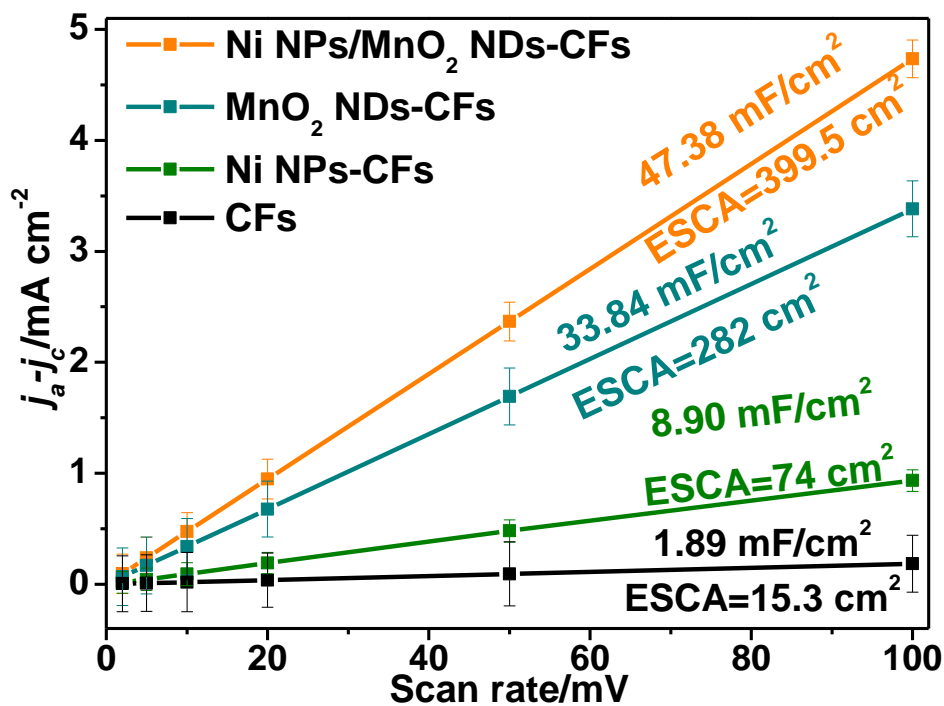


**Figure S13.** Charging current density differences  $j_a-j_c$  plotted against scan rates of the Ni NPs/MnO<sub>2</sub> NDs-CFs, MnO<sub>2</sub> NDs-CFs, Ni NPs-CFs and CFs electrocatalysts.

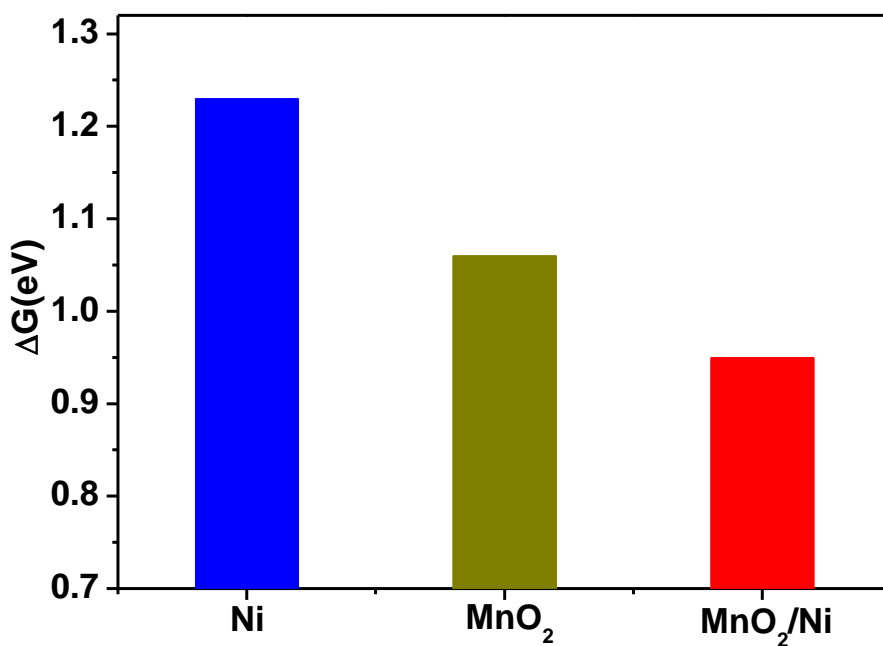


**Figure S14.** DFT calculations of MnO<sub>2</sub>, Ni and MnO<sub>2</sub>/Ni for the free energy barrier of equation (1).

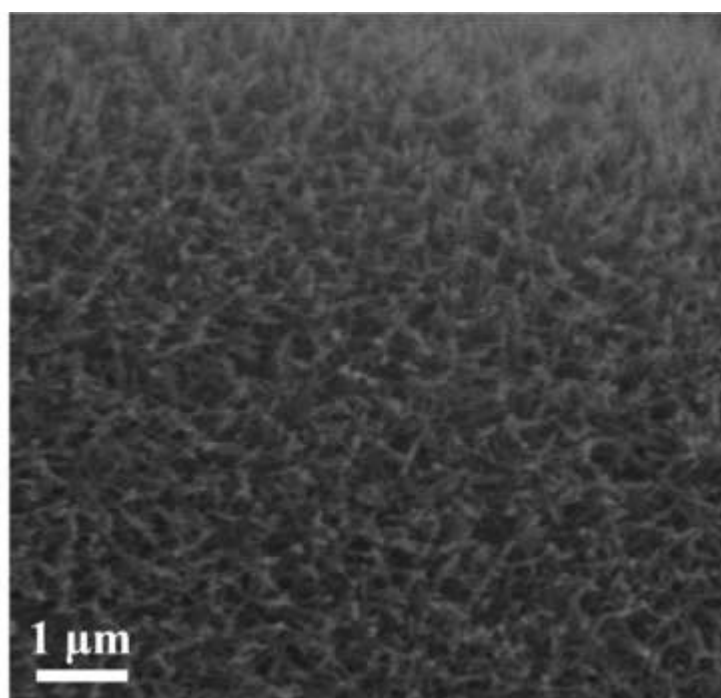


**Figure S15.** SEM image of Ni NPs/MnO<sub>2</sub> NDs-CFs after 40000 s at -0.84 V *vs.* RHE.

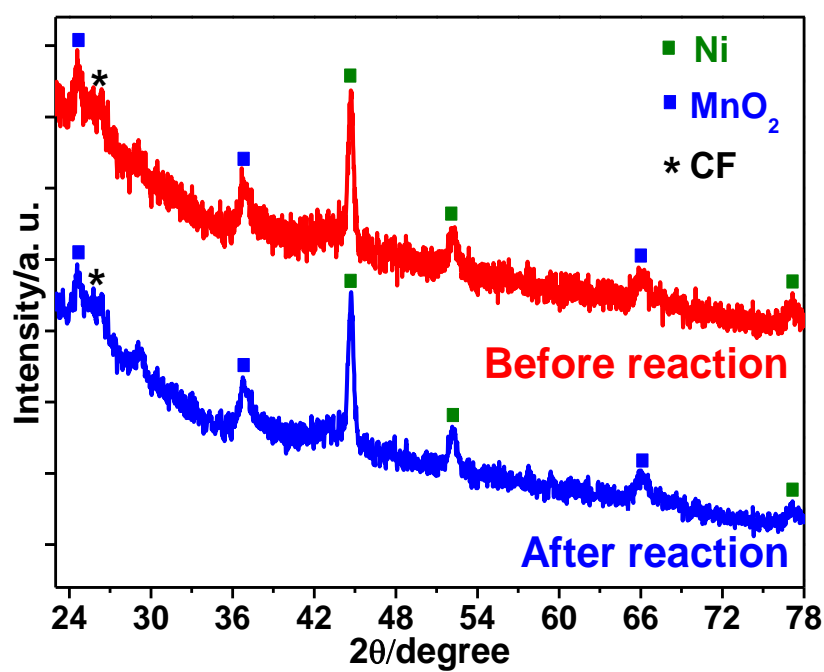


**Figure S16.** XRD patterns of Ni NPs/MnO<sub>2</sub> NDs-CFs before and after 40000 s at -0.84 V *vs.* RHE.

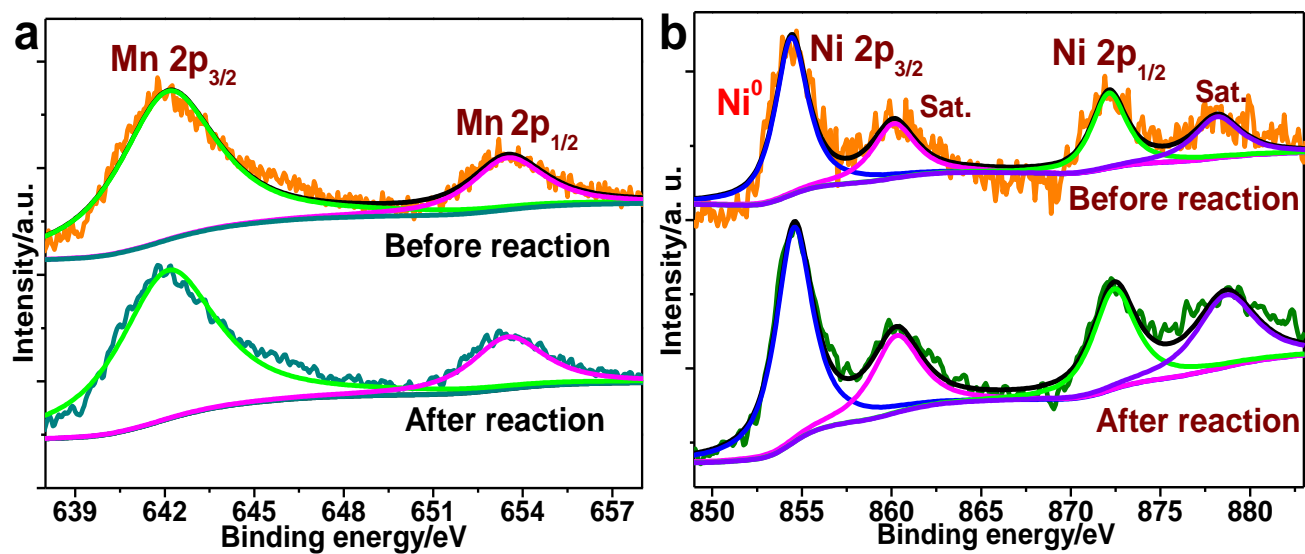


**Figure S17.** XPS spectrum of (a) Mn 2p and (b) Ni 2p of Ni NPs/MnO<sub>2</sub> NDs-CFs before and after 40000 s reaction under -0.84 V vs. RHE.

**Table S1.** Comparison of the electrocatalytic activity of Ni NPs/MnO<sub>2</sub> NDs-CFs catalysts with some representative solid-state CO<sub>2</sub> electrochemical reduction catalysts recently reported. (*U*: Overpotential vs. CO<sub>2</sub>/HCOO<sup>-</sup>; *j*: Current density at the applied overpotential; *FE*: Faradaic efficiency of formate formation)

Catalyst	<i>U</i> /mV	<i>j</i> /mA cm <sup>-2</sup>	<i>FE</i> /%	Reaction time/s	Reference
<b>Ni NPs/MnO<sub>2</sub> NDs-CFs</b>	<b>230</b>	<b>7.25</b>	<b>85.5</b>	<b>100000</b>	<b>Our work</b>
Sn/SnO <sub>x</sub>	390	0.60	19	43200	Ref 1
Pd nanoparticles decorated CNT	200	1.0	65	9000	Ref 3
Partly reduced Co <sub>3</sub> O <sub>4</sub>	240	10.6	91	216000	Ref 7
Cu <sub>2</sub> O film	450	7.5	40	3600	Ref 9
Ultrathin Co <sub>3</sub> O <sub>4</sub>	270	0.68	64.3	144000	Ref 11
N-CNT+polyethylenimine	850	3.0	83	86400	Ref 12
5 nm Sn	340	5.2	93	64800	Ref 18

\*The above references have been listed in paper.